Astronomy & Astrophysics manuscript no. 11867
November 18, 2009
© ESO 2009

arXiv:0910.4027v3 [astro-ph.SR] 18 Nov 2009

The CoRoT⋆ target HD 49933:

1 - Effect of the metal abundance on the mode excitation rates

R. Samadi[1], H.-G. Ludwig[2], K. Belkacem[1,3], M.J. Goupil[1], and M.-A. Dupret[1,3]

[1] Observatoire de Paris, LESIA, CNRS UMR 8109, Université Pierre et Marie Curie, Université Denis Diderot, 5 pl. J. Janssen, F-92195 Meudon, France
[2] Observatoire de Paris, GEPI, CNRS UMR 8111, 5 pl. J. Janssen, F-92195 Meudon, France
[3] Institut d'Astrophysique et de Géophysique de l'Université de Liège, Allée du 6 Août 17 – B 4000 Liège, Belgium

November 18, 2009

ABSTRACT

Context. Solar-like oscillations are stochastically excited by turbulent convection at the surface layers of the stars.
Aims. We study the role of the surface metal abundance on the efficiency of the stochastic driving in the case of the CoRoT target HD 49933.
Methods. We compute two 3D hydrodynamical simulations representative – in effective temperature and gravity – of the surface layers of the CoRoT target HD 49933, a star that is rather metal poor and significantly hotter than the Sun. One 3D simulation has a solar metal abundance, and the other has a surface iron-to-hydrogen, [Fe/H], abundance ten times smaller. For each 3D simulation we match an associated global 1D model, and we compute the associated acoustic modes using a theoretical model of stochastic excitation validated in the case of the Sun and α Cen A.
Results. The rate at which energy is supplied per unit time into the acoustic modes associated with the 3D simulation with [Fe/H]=-1 is found to be about three times smaller than those associated with the 3D simulation with [Fe/H]=0. As shown here, these differences are related to the fact that low metallicity implies surface layers with a higher mean density. In turn, a higher mean density favors smaller convective velocities and hence less efficient driving of the acoustic modes.
Conclusions. Our result shows the importance of taking the surface metal abundance into account in the modeling of the mode driving by turbulent convection. A comparison with observational data is presented in a companion paper using seismic data obtained for the CoRoT target HD 49933.

Key words. convection - turbulence - atmosphere - Stars: oscillations - Stars: individual: HD 49933 - Sun: oscillations

1. Introduction

Using the measured linewidths and the amplitudes of the solar acoustic modes, it has been possible to infer the rate at which energy is supplied per unit time into the solar acoustic modes. Using these constraints, different models of mode excitation by turbulent convection have been extensively tested in the case of the Sun (see e.g. recent reviews by Samadi et al. (2008b) and Houdek (2006)). Among the different approaches, we can distinguish pure theoretical approaches (e.g. Samadi & Goupil 2001; Chaplin et al. 2005), semi-analytical approaches (e.g. Samadi et al. 2003b,a) and pure numerical approaches (e.g. Nordlund & Stein 2001; Stein et al. 2004; Jacoutot et al. 2008). The advantage of a theoretical approach is that it easily allows massive computation of the mode excitation rates for a wide variety of stars with different fundamental parameters (e.g. effective temperature, gravity) and different surface metal abundance. However, pure theoretical approaches are based on crude or simplified descriptions of turbulent convection. On the other hand, a semi-analytical approach is generally more realistic since the quantities related to turbulent convection are obtained from 3D hydrodynamical simulation. 3D hydrodynamical simulations are at this point in time too time consuming, so that a fine grid of 3D models with a sufficient resolution in effective temperature ($T_{\rm eff}$), gravity ($\log g$) and surface metal abundance (Z) is not yet available. In the present paper, we study and provide a procedure to interpolate for any value of Z the mode excitation rates $\mathcal{P}$ between two 3D simulations with different Z but the same $T_{\rm eff}$ and $\log g$. With such interpolation procedure it is no longer required to have at our disposal a fine grid in Z of 3D simulations.

The semi-analytical mode that we consider here is based on Samadi & Goupil (2001)'s theoretical model with the improvements proposed by Belkacem et al. (2006a). This semi-analytical model satisfactorily reproduces the solar seismic data (Samadi et al. 2003a; Belkacem et al. 2006b). Recently, the seismic constraints obtained for α Cen A (HD 128620) have provided an additional validation of the basic physical assumptions of this theoretical model (Samadi et al. 2008a). The star α Cen A has a surface gravity ($\log g = 4.305$) lower than that of the Sun ($\log\ g_\odot = 4.438$), but its effective temperature ($T_{\rm eff} = 5810$ K) does not significantly differ from that of the Sun ($T_{\rm eff,\odot} = 5780$ K). The higher $T_{\rm eff}$, the more vigorous the

⋆ The CoRoT space mission, launched on December 27 2006, has been developped and is operated by CNES, with the contribution of Austria, Belgium, Brasil, ESA, Germany and Spain.
Correspondence to: Reza.Samadi@obspm.fr

convective velocity at the surface and the stronger the driving by turbulent convection (see e.g. Houdek et al. 1999). For main sequence stars with a mass $M \lesssim 1.6\,M_\odot$, an increase of the convective velocity is expected to be associated with a larger turbulent Mach number, M_t (Houdek et al. 1999). However, the theoretical models of stochastic excitation are strictly valid in a medium where M_t is – as in the Sun and α Cen A – rather small. Hence, the higher M_t, the more questionable the different approximations and the assumptions involved in the theory (see e.g. Samadi & Goupil 2001). It is therefore important to test the theory with another star characterized by a $T_{\rm eff}$ significantly higher than in the Sun.

Furthermore, the star α Cen A has an iron-to-hydrogen abundance slightly larger than the Sun, namely [Fe/H]= 0.2 (see Neuforge-Verheecke & Magain 1997). However, the modeling performed by Samadi et al. (2008a) for α Cen A assumes a solar iron abundance ([Fe/H]=0). According to Houdek et al. (1999), the mode amplitudes are expected to change with the metal abundance. However, Houdek et al. (1999)'s result was obtained on the basis of a mixing-length approach involving several free parameters and by using a theoretical model of stochastic excitation in which a free multiplicative factor is introduced in order to reproduce the maximum of the solar mode excitation rates. Therefore, it is important to extend Houdek et al. (1999)'s study by using a more realistic modeling based on 3D hydrodynamical simulation of the surface layers of stars and a theoretical model of mode driving that reproduces – without the introduction of free parameters – the available seismic constraints.

To this end, the star HD 49933 is an interesting case for three reasons: First, this star has $T_{\rm eff} = 6780 \pm 130$ K (Bruntt et al. 2008), $\log g \simeq 4.25 \pm 0.13$ (Bruntt et al. 2008) and [Fe/H] $\simeq -0.37$ dex (Solano et al. 2005; Gillon & Magain 2006). The properties of its surface layers are thus significantly different from those of the Sun and α Cen A. Second, HD 49933 was observed in Doppler velocity with the HARPS spectrograph. A seismic analysis of these data performed by Mosser et al. (2005) has provided the maximum of the mode surface velocity ($V_{\rm max}$). Third, the star was more recently observed continuously in intensity by CoRoT during 62 days. Apart from observations for the Sun, this is the longest seismic observation ever peformed both from the ground and from space. This long term and *continuous* observation provides a very high frequency resolution ($\sim 0.19\,\mu$Hz). The seismic analysis of these observations undertaken by Appourchaux et al. (2008) or more recently by Benomar et al. (2009) have provided the *direct* measurements of the mode amplitudes and the mode linewidths with an accuracy not previously achieved for a star other than the Sun.

We consider two 3D hydrodynamical simulations representative – in effective temperature and gravity – of the surface layers of HD 49933. One 3D simulation has [Fe/H]=0, while the second has [Fe/H]= -1. For each 3D simulation, we match an associated global 1D model and compute the associated acoustic modes and mode excitation rates, $\mathcal{P}$. This permits us to quantify the variation of $\mathcal{P}$ induced by a change of the surface metal abundance Z. From these two sets of calculation, we then deduce $\mathcal{P}$ for HD 49933 by taking into account the observed iron abundance of the star (i.e. [Fe/H]=-0.37). In a companion paper (Samadi et al. 2009, hereafter Paper II), we will use these theoretical calculations of $\mathcal{P}$ and the mode linewidths obtained from the seismic analysis of HD 49933 performed with the CoRoT data to derive the expected mode amplitudes in HD 49933. These computed mode amplitudes will then be compared with the observed ones. This comparison will then constitute a test of the stochastic excitation model with a star significantly different from the Sun and α Cen A. It will also constitute a test of the procedure proposed here for deriving $\mathcal{P}$ for any value of Z between two 3D simulations with different Z.

The present paper is organised as follows: we first describe in Sect. 2 the method to compute the theoretical mode excitation rates associated with the two 3D hydrodynamical simulations. Next, the effects on $\mathcal{P}$ of a different surface metal abundance are presented in Sect. 3. Then, by taking into account the actual iron abundance of HD 49933, we derive theoretical values of $\mathcal{P}$ expected for HD 49933. Finally, Sect. 5 is dedicated to our conclusions.

2. Calculation of mode excitation rates

2.1. Model of stochastic excitation

The energy injected into a mode per unit time $\mathcal{P}$ is given by the relation (see Samadi & Goupil 2001; Belkacem et al. 2006b):

$$\mathcal{P} = \frac{1}{8\,I}\left(C_R^2 + C_S^2\right)\ , \tag{1}$$

where C_R^2 and C_S^2 are the turbulent Reynolds stress and entropy contributions, respectively, and

$$I = \int_0^M {\rm dm}\,|\xi_r|^2 \tag{2}$$

is the mode inertia, ξ_r is the adiabatic radial mode displacement and M is the mass of the star. The expressions for C_R^2 and C_S^2 are given for a radial mode with frequency $\omega_{\rm osc}$ by

$$C_R^2 \ = \ \frac{64\pi^3}{15}\int {\rm dm}\,\frac{\bar\rho\,\tilde u^4}{k_0^3\,\omega_0}\,\frac{\mathcal{K}_w}{3}\,f_r\,S_R(r,\omega_{\rm osc})\ , \tag{3}$$

$$C_S^2 \ = \ \frac{16\pi^3}{3\,\omega_{\rm osc}^2}\int {\rm dm}\,\frac{(\alpha_s\,\tilde s\,\tilde u)^2}{\bar\rho\,k_0^3\,\omega_0}\,g_r\ S_s(r,\omega_{\rm osc}) \tag{4}$$

where we have defined the "source functions":

$$S_R(r,\omega_{\rm osc}) \ = \ \frac{k_0^3\,\omega_0}{\tilde u^4}\int\frac{{\rm d}k}{k^2}\,E^2(k) \times\int {\rm d}\omega\,\chi_k(\omega+\omega_{\rm osc})\ \chi_k(\omega) \tag{5}$$

$$S_s(r,\omega_{\rm osc}) \ = \ \frac{k_0^3\,\omega_0}{\tilde u^2\,\tilde s^2}\int\frac{{\rm d}k}{k^2}\,E(k)\,E_s(k) \times\int {\rm d}\omega\,\chi_k(\omega+\omega_{\rm osc})\,\chi_k(\omega) \tag{6}$$

where P is the gas pressure, ρ the density, s the entropy, $\bar\rho$ the equilibrium density profile, $\alpha_s \equiv (\partial P/\partial s)_\rho$, $f_r \equiv ({\rm d}\xi_r/{\rm d}r)^2$ and g_r are two functions that involve the first and second derivatives of ξ_r respectively, k is the wavenumber, $E(k)$ is the turbulent kinetic energy spectrum, $E_s(k)$ is the spectrum associated with the entropy fluctuations (s), $\tilde s$ is the rms of s, χ_k is the time-correlation function associated with the velocity, $\tilde u$ is a characteristic velocity defined in a way that $3\,\tilde u^2 = \langle \boldsymbol{u}^2\rangle$, $\langle . \rangle$ refers to horizontal

and time average, $\boldsymbol{u}$ is the turbulent velocity field, and finally $\mathcal{K}_w \equiv \langle u_z^4 \rangle / \langle u_z^2 \rangle^2$ is the Kurtosis (see Belkacem et al. 2006a,b, for details). Furthermore, we have introduced for convenience the characteristic frequency ω_0 and the characteristic wavenumber k_0:

$$\omega_0 \equiv k_0 \, \tilde{u} \tag{7}$$

$$k_0 \equiv \frac{2\pi}{\Lambda} \tag{8}$$

where Λ is a characteristic size derived from $E(k)$ as explained in Samadi et al. (2003b). Note that the introduction of the term $k_0^3 \, \omega_0 \, \tilde{u}^{-4}$ in the RHS of Eq. (5) and the term $k_0^3 \, \omega_0 \, \tilde{u}^{-2} \, \tilde{s}^{-2}$ in the RHS of Eq. (6) ensure dimensionless source functions.

The kinetic spectrum $E(k)$ is derived from the 3D simulation as detailled in Samadi et al. (2003b). As shown by Samadi et al. (2003b), the k-dependence of $E_s(k)$ is similar to that of the $E(k)$. Accordingly, we assume $E_s \propto E$.

In Samadi et al. (2008a), two different analytical functions for $\chi_k(\omega)$ have been considered, namely a Lorentzian function and a Gaussian one. In the present study we will in addition derive $\chi_k(\omega)$ *directly* from the 3D simulations as detailled in Samadi et al. (2003a). Once $\chi_k(\omega)$ is derived from the 3D simulation, it is implemented in Eq. (5) and Eq. (6).

We compute the mode excitation as detailled in Samadi et al. (2008a): all required quantities – except ξ_r, I and $\omega_{\rm osc}$ – are obtained *directly* from two 3D hydrodynamical simulations representative of the outer layers of HD 49933, whose characteristics are described in Sect. 2.2 below.

The quantities related to the modes ($\omega_{\rm osc}$, I and $\xi_{\rm r}$) are calculated using the adiabatic pulsation code ADIPLS (Christensen-Dalsgaard & Berthomieu 1991) from 1D global models. The outer layers of these 1D models are derived from the 3D simulation as described in Sect. 2.3.

2.2. The 3D simulations

We computed two 3D radiation-hydrodynamical model atmospheres with the code CO^{5}BOLD (Freytag et al. 2002; Wedemeyer et al. 2004). One 3D simulation had a solar iron-to-hydrogen [Fe/H]=0.0 while the other had [Fe/H]=-1.0. The 3D model with [Fe/H]=0 (resp. [Fe/H]=-1) will be hereafter referred to as model S0 (resp. S1). The assumed chemical composition is similar (in particular for the CNO elements) to that of the solar chemical composition proposed by Asplund et al. (2005). The abundances of the α-elements in model S1 were assumed to be enhanced by 0.4 dex. For S0 we obtain $Z/X = 0.01830$ and Y=0.249, and for S1 $Z/X = 0.0036765$ and Y=0.252. Both 3D simulations have exactly the same gravity ($\log g$ =4.25) and are very close in effective temperature ($T_{\rm eff}$). Both models employ a spatial mesh with $140 \times 140 \times 150$ grid points, and a physical extent of the computational box of $16.4 \times 16.4 \times 24.2$ Mm^3. The equation of state takes into account the ionisation of hydrogen and helium as well as the formation of H_2 molecules according to the Saha-Boltzmann statistics. The wavelength dependence of the radiative transfer is treated by the opacity binning method (Nordlund 1982; Ludwig 1992; Vögler et al. 2004) using five wavelength bins for model S0 and six for model S1. Detailed wavelength-dependent opacities were obtained from the MARCS model atmosphere package (Gustafsson et al. 2008). Table 1 summarizes the characteristics of the 3D models. The effective temperature and surface gravity correspond to the parameters of HD 49933 within the observational uncertainties, while the two metallicities bracket the observed value.

For each 3D simulation, two time series were built. One has a long duration (38h and 20h for S0 and S1, respectively) and a low sampling frequency (10 mn). This time series is used to compute time averaged quantities ($\bar{\rho}$, $E(k)$, etc.). The second time series is shorter (8.8h and 6.8h for S0 and S1, respectively), but has a high sampling frequency (1 mn). Such high sampling frequency is required for the calculation of $\chi_k(\omega)$. Indeed, the modes we are looking at lie between $\nu \approx 1.25$ mHz and $\nu \approx 2.4$ mHz.

Label	[Fe/H]	Y	Z	Z/X	$T_{\rm eff}$ [K]
S0	0	0.249	$13.5\ 10^{-3}$	0.018305	6725 ± 17
S1	-1	0.252	$2.74\ 10^{-3}$	0.003676	6730 ± 12

Table 1. Characteristics of the 3D simulations.

The two 3D simulations extend up to $T = 100\,000$ K. However, for $T \gtrsim 30\,000$ K, the 3D simulations are not completely realistic. First of all, the MARCS-based opacities are provided only up to a temperature of 30 000 K; for higher temperatures the value at 30 000 K is assumed. Note that we refer to the opacity per unit mass here. For the radiative transfer the opacity per unit volume is the relevant quantity, i.e. the product of opacity per mass unit and density. Since in the simulation the opacity is still multiplied at each position with the correct local density, the actual error we make when extrapolating the opacity is acceptable.

Another limitation of the simulations is the restricted size of the computational box which does not allow for a full development of the largest flow structures, again in the layers above $T \simeq 30\,000$ K. Two hints make us believe that the size of the computational domain is not fully sufficient: i) in the deepest layers of the simulations there is a tendency that structures align with the computational grid; ii) the spatial spectral power P of scalar fields in a horizontal layer does not tend towards the expected asymptotic behaviour $P \times k$ for low spatial wavenumber k. We noticed this shortcoming only after the completion of the simulation runs. To mitigate its effect in our analysis, we will later by default integrate the mode excitation rates up to $T = 30\,000$ K. However, for comparison purposes, some computations have been extended down to the bottom of the 3D simulations. For S0, the layers located below $T \simeq 30\,000$ K contribute only by $\lesssim 10\,\%$ to the excitation of the modes lying in the frequency range where modes have the most chance to be detected ($\nu \simeq 1.2 - 2.5$ mHz). For S1, the contribution of the deep layers is even smaller ($\sim 5\,\%$).

Finally, one may wonder how the treatment of the small-scales or the limited spatial resolution of the simulation can influence our calculations. Dissipative processes are handled in CO^{5}BOLD on the one hand side implicitely by the numerical scheme (Roe-type approximate Riemann solver), and on the other hand explicitely by a sub-grid model according to the classical Smagorinsky (1963) formulation. Jacoutot et al. (2008) found that computed mode excitation rates significantly depend on the adopted sub-grid model. Samadi et al. (2007) have found that solar mode ex-

citation rates computed in the manner of Nordlund & Stein (2001), i.e., using data directly from the 3D simulation, decrease as the spatial resolution of the solar 3D simulation decreases. As a conclusion the spatial resolution or the subgrid model can influence computed mode excitation rates (see a discussion in Samadi et al. 2008a). However, concerning the spatial resolution and according to Samadi et al. (2007)'s results, the present spatial resolution (1/140 of the horizontal size of the box and about 1/150 of the vertical extent of the simulation box) is high enough to obtain accurate computed energy rates. The increased spatial resolution of our models in comparison to the work of Jacoutot et al. (2008) reduces the impact of the unresolved scales.

2.3. The 1D global models

For each 3D model we compute an associated 1D global model. The models are built in the manner of Trampedach (1997) as detailled in Samadi et al. (2008a) in such way that their outer layers are replaced by the averaged 3D simulations described in Sect. 2.2. The interior of the models are obtained with the CESAM code assuming standard physics: Convection is described according to Böhm-Vitense (1958)'s local mixing-length theory of convection (MLT), and turbulent pressure is ignored. Microscopic diffusion is not included. The OPAL equation of state is assumed. The chemical mixture of the heavy elements is similar to that of Asplund et al. (2005)'s mixture. As in Samadi et al. (2008a), we will refer to these models as "patched" models hereafter.

The two models have the effective temperature and the gravity of the 3D simulations. One model is matched with S0 and has [Fe/H]=0, while the second is matched with S1 and has [Fe/H]=-1. The 1D models have the same chemical mixture as their associated 3D simulations. The parameters of the 1D patched models are given in Table 2. The stratification in density and temperature of the patched 1D models are shown in Fig. (1). At any given temperature the density is larger in S1 as a consequence of its lower metal abundance. Indeed, the lower the metal abundance, the lower the opacity ; then, at a given optical depth (τ), the density is larger in S1 compared to S0. The photosphere corresponds to the optical depth $\tau = 2/3$. Since the two 3D simulations have approximatively the same effective temperature, the density in S1 is larger at optical depth $\tau = 2/3$. Since the density in S1 increases with depth even more rapidly than in S0, the density in S1 remains larger for $\tau > 2/3$ than in S0.

3. Effects of the metal abundance on excitation rates

The mode excitation rates ($\mathcal{P}$) are computed for the two 3D simulations according to Eqs. (1)-(6). The integration is performed from the top of the simulated domains down to $T = 30\,000$ K (see Sect. 2.2). In the following, $\mathcal{P}_1$ (resp. $\mathcal{P}_0$) corresponds to the mode excitation rates associated with the 3D model with [Fe/H]=-1 (resp. [Fe/H]=0)

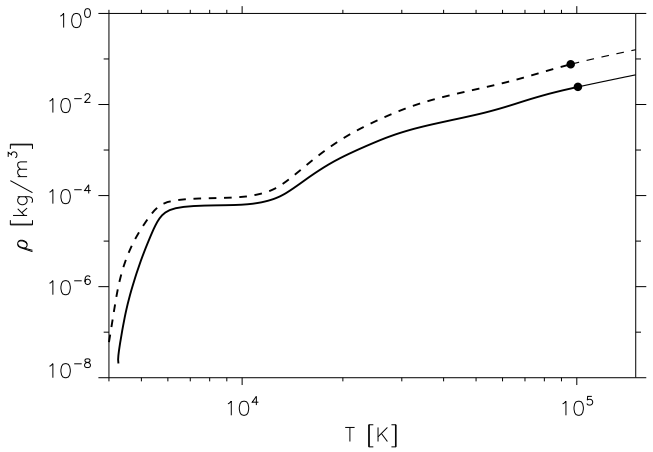

Fig. 1. Mean density $\bar{\rho}$ as a function of temperature, T. The solid line corresponds to the 3D model with the metal abundance (S0) and the dashed line to metal poor 3D model (S1). The filled dots show the location where the 1D models have been matched to the associated 3D simulation.

3.1. Results

Figure 2 shows the effect of the assumed metal abundance of the stellar model on the mode excitation rates. $\mathcal{P}_1$ is found to be three times smaller than $\mathcal{P}_0$, i.e. p modes associated with the metal poor 3D model (S1) receive approximatively three times less energy per unit time than those associated with the 3D model with the solar metal abundance (S0).

For both 3D models, the dominant part of the driving is ensured by the Reynolds stresses. The entropy fluctuations contribute by only $\sim$ 30 % of the total power for both S0 and S1. By comparison, in the case of the Sun and α Cen A it contributes by only $\sim$ 15 %. Furthermore, we find that the contribution of the entropy source term is – as for the Reynolds stress term – about three times smaller in S1 than in S0. We conclude that the effect of the metal abundance on the excitation rates is almost the same for the Reynolds stress contribution and the entropy source term.

3.2. Interpretation

From Eqs. (1), (2), (3), (7) and (8) we show that at a given layer the power supplied to the modes – per unit mass – by the *Reynolds stress* is proportional to $F_{\rm kin}\,\Lambda^4\,S_R/\mathcal{M}$, where $F_{\rm kin}$ is the flux of the kinetic energy, which is proportional to $\bar{\rho}\,\tilde{u}^3$, Λ is a characteristic length (see Sect. 2.1) and $\mathcal{M}$ is the mode mass defined as:

$$\mathcal{M} = \frac{I}{\xi_r^2} \tag{9}$$

where ξ_r is the mode displacement evaluated at the layer in the atmosphere where the mode is measured.

The power supplied to the modes – per unit mass – by the entropy source term is proportional to $\bar{\rho}\,\tilde{u}^3\,\Lambda^4\,\mathcal{R}^2\,S_s$ where $\omega_{\rm osc}$ is the mode frequency, $\mathcal{R} \propto F_{\rm conv}/F_{\rm kin}$, where $F_{\rm conv} \propto w\,\alpha_s\,\tilde{s}$ is the convective flux, and finally $\tilde{s}$ is the rms of the entropy fluctuations (see Samadi et al. 2006). We recall that the higher $\mathcal{R}$, the higher the *relative* contribution of the entropy source to the excitation. We study below the role of $\mathcal{M}$, $F_{\rm kin}$, Λ, S_R, S_s and $\mathcal{R}$:

[Fe/H]	Y	Z	$T_{\rm eff}$ [K]	$R/R_\odot$	$M/M_\odot$	α
0	0.249	$13.5\ 10^{-3}$	6726	1.473	1.408	1.677
-1	0.252	$2.74\ 10^{-3}$	6732	1.261	1.033	1.905

Table 2. Characteristics of the 1D "patched" models. α is the mixing-length parameter.

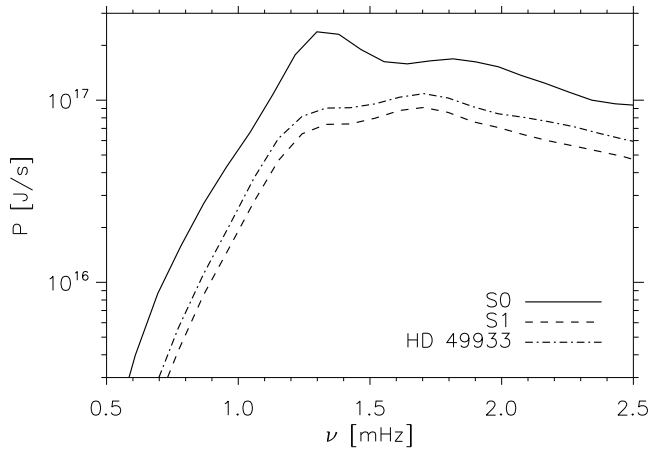

Fig. 2. Mode excitation rates $\mathcal{P}$ as a function of the mode frequency, ν. The solid line corresponds to the 3D model with the canonical metal abundance (S0) and the dashed line to the metal poor 3D model (S1). The dot-dashed line corresponds to the mode excitation rates derived for the specific case of HD 49933 as explained in Appendix A.

Mode mass ($\mathcal{M}$): The frequency domain, where modes are strongly excited, ranges between $\nu \approx 1.2$ mHz and $\nu \approx 2.5$ mHz. In this frequency domain, the mode masses $\mathcal{M}$ associated with S0 are quite similar to those associated with S1 (not shown). Consequently the differences between $\mathcal{P}_1$ and $\mathcal{P}_0$ do not arise from the (small) differences in $\mathcal{M}$.

Kinetic energy flux ($F_{\rm kin}$): The larger $F_{\rm kin}$, the larger the driving by the Reynolds stress. However, we find that the two 3D models have very similar $F_{\rm kin}$. This is not surprising since the two 3D models have very similar effective temperatures. This means that the differences between $\mathcal{P}_1$ and $\mathcal{P}_0$ do not arise from the (small) differences in $F_{\rm kin}$.

Characteristic length (Λ): In the manner of Samadi et al. (2003b) we derive from the kinetic energy spectra $E(k)$ of the two 3D simulations the characteristic length Λ ($\Lambda = 2\pi/k_0$, see Eq. (8)) for each layer of the simulated domain. We find that the differences in Λ between the two 3D simulations is small and does not play a significant role in the differences in $\mathcal{P}$. This can be understood by the fact that S0 and S1 have the same gravity. Indeed, as shown by Samadi et al. (2008a) – at a fixed effective temperature – Λ scales as the inverse of g. We conclude that the differences between $\mathcal{P}_1$ and $\mathcal{P}_0$ do not originate from the (small) differences in Λ.

Source functions (S_R and S_s): The dimensionless source functions S_R and S_s are defined in Eqs. (5) and (6) respectively. Both source functions involve the eddy time-correlation function $\chi_k(\omega)$. We define ω_k as the frequency width of $\chi_k(\omega)$. As shown by Samadi et al. (2003a) and as verified in the present case, ω_k can be evaluated as the product $k\,u_k$ where u_k is given by the relation (Stein 1967):

$$u_k^2 = \int_k^{2k} {\rm d}k\, E(k) \tag{10}$$

where $E(k)$ is normalised as:

$$\int_0^{+\infty} {\rm d}k\, E(k) \ = \tfrac{1}{2}\langle u^2\rangle \equiv \tfrac{1}{2}\tilde{u}^2\ . \tag{11}$$

According to Eqs. (10) and (11), u_k is directly proportional to $\tilde{u}$. At a fixed k/k_0, we then have $\omega_k \propto \tilde{u}\,k_0 = \omega_0$.

As seen above, ω_0 controls ω_k, the frequency width of χ_k. Then, at fixed $\omega_{\rm osc}$, we can easly see from Eqs. (5) and (6) that the smaller ω_0, the smaller $S_R(\omega_{\rm osc})$ and $S_s(\omega_{\rm osc})$. Since $\omega_0 = \tilde{u}\,k_0 = 2\pi\,\tilde{u}/\Lambda$ and since both 3D simulations have approximately the same Λ, smaller $\tilde{u}$ results directly in smaller ω_0 and hence in smaller source functions.

We have plotted in Fig. 3 the characteristic velocity $\tilde{u}$. This quantity is found to be up to 15 % smaller for S1 compared with S0. In other words, the metal poor 3D model is characterized by lower convective velocities. Consequently, the source functions are smaller for S1 compared to S0. Although the convective velocities differ between S0 and S1 by only 15 %, the excitation rates differ by a factor ~ 3. The reason for this is that he source functions, which are non-linear functions of $\tilde{u}$, decrease very rapidly with $\tilde{u}$. This is the consequence of the behavior of the eddy-time correlation χ_k. Indeed, this function varies with the ratio $\omega_{\rm osc}/\omega_k$ approximately as a Lorentzian function. This is why χ_k varies rapidly with $\tilde{u}$ (we recall that $\omega_k \propto \tilde{u}\,k_0$).

In conclusion, the differences between $\mathcal{P}_1$ and $\mathcal{P}_0$ are mainly due to differences in the characteristic velocity $\tilde{u}$. In turn, the low convective velocity in S1 is a consequence of the larger density compared to S0. Indeed, as shown in Fig. 1, the density is systematically higher in S1. At the layer where the modes are the most excited (i.e. at $T \sim 10000K$), the density is ~ 50 % higher. Since the two 3D models have a similar kinetic energy flux (see above), it follows that a larger density for S1 then implies lower convective velocities.

Relative contribution of the entropy source term ($\mathcal{R}$): The convective flux $F_{\rm conv}$ in S1 is almost identical to that of S0. This is due to the fact that the two 3D simulations have almost the same effective temperature. Furthermore, as pointed out above, the differences in $F_{\rm kin}$ between S1 and S0 are small. As a consequence, the ratio $\mathcal{R} \propto F_{\rm conv}/F_{\rm kin}$ does not differ between the two 3D simulations. Accordingly, as for the Reynolds contribution, the variation of the excitation rates with the metal abundance is only due to the source term S_S. The latter varies with ω_0 in the same manner as S_R, which is turn the reason for As a consequence, the contribution of the entropy fluctuations to show the same trend with the metal abundance as the Reynolds stress term.

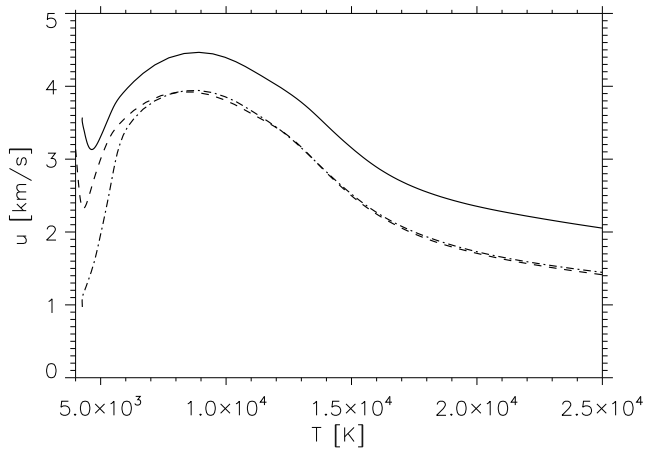

Fig. 3. Characteristic velocity $\tilde{u}$ defined in Eq. (7) as a function of temperature, T. The solid and dashed lines have the same meaning as in Fig. 2. The dot-dashed line corresponds to the solid line multiplied by γ_1, where $\gamma_1(T) \equiv (\bar{\rho}_0/\bar{\rho}_1)^{1/3}$ and $\bar{\rho}_0$ (resp. $\bar{\rho}_1$) is the mean density stratification of S0 (resp. S1)(see Appendix A).

4. Theoretical calculation of $\mathcal{P}$ for HD 49933

We derive the mode excitation rates $\mathcal{P}$ for HD 49933. According to Gillon & Magain (2006), HD 49933 has [Fe/H]=-0.37 ± 0.03 dex, while we only have two 3D simulations with values of [Fe/H], respectively [Fe/H]=0 and [Fe/H]=-1.

As seen in Sect. 3.2, differences in $\mathcal{P}$ between S0 and S1 are a direct consequence of the differences in the source functions S_R and S_S. It follows that in order to derive $\mathcal{P}$ for HD 49933, we only have to derive the expected values for S_R and S_S. As seen in Sect. 3.2, differences in S_R (or in S_S) between S0 and S1 are related to the surface metal abundance through the surface densities that impact the convective velocities ($\tilde{u}$). The determination of the HD 49933 convective velocities allows us to determine its source function. To this end, we use the fact that the kinetic flux is almost unchanged between S1 and S0 (see Sect. 3.2) to derive the profile of $\tilde{u}(T)$, expected at the surface layers of HD 49933. This is performed by interpolating in Z between S0 and S1, the surface density stratification representative of the surface layers of HD 49933. The whole procedure is described in Appendix A.

In order to compute $\mathcal{P}$ for HD 49933, we then need to know Z for this star. Since we do not know its surface helium abundance, we will assume by default the solar value for Y: $Y = 0.249 \pm 0.003$ (Basu 1997). Gillon & Magain (2006)'s analysis shows that the chemical mixture of HD 49933 does not significantly differ from that of the Sun. According to Asplund et al. (2005), the new solar metal to hydrogen ratio is $(Z/X)_\odot = 0.0165$ Accordingly, since [Fe/H]=- 0.37 ± 0.03 dex, we derive $Z = 5.3\ 10^{-3} \pm 0.4\,10^{-3}$ for HD 49933. Note that assuming Grevesse & Noels (1993)'s chemical mixture yields $Z = 7.8\ 10^{-3} \pm 0.5\ 10^{-3}$.

The result of the calculation is shown in Fig. 2. The maximum $\mathcal{P}$ is $1.08 \pm 0.05\ 10^{17}$ J/s when Asplund et al. (2005)'s chemical composition is assumed (see Appendix A). This is about 30 times larger than in the Sun and about 14 times larger than in α Cen A. When Grevesse & Noels (1993)'s chemical mixture is assumed, the maximum in $\mathcal{P}$ is in that case equal to $1.27 \pm 0.05\ 10^{17}$J/s, that is about 30 % larger than with Asplund et al. (2005)'s solar chemical mixture.

We note that the uncertainties in the knowledge of [Fe/H] set uncertainties on $\mathcal{P}$ which are the on order of 10 % in the frequency domain of interest.

5. Conclusion

We have built two 3D hydrodynamical simulations representative in effective temperature ($T_{\rm eff}$) and gravity (g) of the surface layers of an F type star on the main sequence. One model has a solar iron-to-hydrogen abundance ([Fe/H]=0) and the other has [Fe/H]=-1. Both models have the same $T_{\rm eff}$ and g. For each 3D simulation, we have computed an associated "patched" 1D full model. Finally, we have computed the mode excitation rates $\mathcal{P}$ associated with the two "patched" 1D models.

Mode excitation rates associated with the metal poor 3D simulation are found to be about three times smaller than those associated with the 3D simulation which has a solar surface metal abundance. This is explained by the following connections: the lower the metallicity, the lower the opacity. At fixed effective temperature and surface gravity, the lower the opacity, the denser the medium at a given optical depth. The higher the density, the smaller are the convective velocities to transport the same amount of energy by convection. Finally, smaller convective velocities result in a less efficient driving. On the other hand, a surface metal abundance higher than the solar metal abundance will result in a lower surface density, which in turn will result in a higher convective velocity and then in a more efficient driving. Our result can then be qualitatively generalised for any surface metal abundance.

By taking into account the observed surface metal abundance of the star HD 49933 (i.e. [Fe/H]=-0.37), we have derived, using two 3D simulations and the interpolation procedure developed here, the rates at which acoustic modes are expected to be excited by turbulent convection in the case of HD 49933. These excitation rates $\mathcal{P}$ are found to be about two times smaller than for a model built assuming a solar metal abundance. These theoretical mode excitation rates will be used in Paper II to derive the expected mode amplitudes from measured mode linewidths. We will then be able to compare these amplitudes with those derived for HD 49933 from different seismic data. This will constitute an indirect test of our procedure which permits us to interpolate for any value of Z the mode excitation rates $\mathcal{P}$ between two 3D simulations with different Z but the same $T_{\rm eff}$ and $\log g$. We must stress that a more direct validation of this interpolation procedure will be to compute a third 3D model with the surface metal abundance of the star HD 49933 and to compare finally the mode excitation rates obtained here with the interpolation procedure with that obtained with this third 3D model. This represents a long term work since several months (about three to four months) are required for the calculation of this additional 3D model, which is in progress.

Acknowledgements. We thank C. Catala for useful discussions concerning the spectrometric properties of HD 49933. We are indebted to

J. Leibacher for his careful reading of the manuscript. K.B. acknowledged financial support from Liège University through the Subside Fédéral pour la Recherche 2009.

References

Appourchaux, T., Michel, E., Auvergne, M., et al. 2008, A&A, 488, 705
Asplund, M., Grevesse, N., & Sauval, A. J. 2005, in Astronomical Society of the Pacific Conference Series, Vol. 336, Cosmic Abundances as Records of Stellar Evolution and Nucleosynthesis, ed. T. G. Barnes, III & F. N. Bash, 25
Basu, S. 1997, MNRAS, 288, 572
Belkacem, K., Samadi, R., Goupil, M. J., & Kupka, F. 2006a, A&A, 460, 173
Belkacem, K., Samadi, R., Goupil, M. J., Kupka, F., & Baudin, F. 2006b, A&A, 460, 183
Benomar, O., Baudin, F., Campante, T., et al. 2009, A&A, 507, L13, arXiv:0910.3060
Böhm-Vitense, E. 1958, Zeitschr. Astrophys., 46, 108
Bruntt, H., De Cat, P., & Aerts, C. 2008, A&A, 478, 487
Chaplin, W. J., Houdek, G., Elsworth, Y., et al. 2005, MNRAS, 360, 859
Christensen-Dalsgaard, J. & Berthomieu, G. 1991, Theory of solar oscillations (Solar interior and atmosphere (A92-36201 14-92). Tucson, AZ, University of Arizona Press, 1991), 401–478
Freytag, B., Steffen, M., & Dorch, B. 2002, Astronomische Nachrichten, 323, 213
Gillon, M. & Magain, P. 2006, A&A, 448, 341
Grevesse, N. & Noels, A. 1993, in Origin and Evolution of the Elements, ed. N. Prantzos, E. Vangioni-Flam, & M. Cassé (Cambridge University Press), 15
Gustafsson, B., Edvardsson, B., Eriksson, K., et al. 2008, A&A, 486, 951
Houdek, G. 2006, in ESA Special Publication, Vol. 624, Proceedings of SOHO 18/GONG 2006/HELAS I, Beyond the spherical Sun, Published on CDROM, p. 28.1
Houdek, G., Balmforth, N. J., Christensen-Dalsgaard, J., & Gough, D. O. 1999, A&A, 351, 582
Jacoutot, L., Kosovichev, A. G., Wray, A. A., & Mansour, N. N. 2008, ApJ, 682, 1386
Ludwig, H.-G. 1992, PhD thesis, University of Kiel
Mosser, B., Bouchy, F., Catala, C., et al. 2005, A&A, 431, L13
Neuforge-Verheecke, C. & Magain, P. 1997, A&A, 328, 261
Nordlund, A. 1982, A&A, 107, 1
Nordlund, Å. & Stein, R. F. 2001, ApJ, 546, 576
Samadi, R., Belkacem, K., Goupil, M. J., Dupret, M.-A., & Kupka, F. 2008a, A&A, 489, 291
Samadi, R., Belkacem, K., Goupil, M.-J., Ludwig, H.-G., & Dupret, M.-A. 2008b, Communications in Asteroseismology, 157, 130
Samadi, R., Georgobiani, D., Trampedach, R., et al. 2007, A&A, 463, 297
Samadi, R. & Goupil, M. . 2001, A&A, 370, 136
Samadi, R., Kupka, F., Goupil, M. J., Lebreton, Y., & van't Veer-Menneret, C. 2006, A&A, 445, 233
Samadi, R., Ludwig, H.-G., Belkacem, K., et al. 2009, A&A, in press, arXiv:0910.4037 (Paper II)
Samadi, R., Nordlund, Å., Stein, R. F., Goupil, M. J., & Roxburgh, I. 2003a, A&A, 404, 1129
Samadi, R., Nordlund, Å., Stein, R. F., Goupil, M. J., & Roxburgh, I. 2003b, A&A, 403, 303
Smagorinsky, J. 1963, Monthly Weather Review, 91, 99
Solano, E., Catala, C., Garrido, R., et al. 2005, AJ, 129, 547
Stein, R., Georgobiani, D., Trampedach, R., Ludwig, H.-G., & Nordlund, Å. 2004, Sol. Phys., 220, 229
Stein, R. F. 1967, Solar Physics, 2, 385
Trampedach, R. 1997, Master's thesis, Master's thesis, Aarhus University (1997)
Vögler, A., Bruls, J. H. M. J., & Schüssler, M. 2004, A&A, 421, 741
Wedemeyer, S., Freytag, B., Steffen, M., Ludwig, H.-G., & Holweger, H. 2004, A&A, 414, 1121

Online Material

Appendix A: Theoretical calculation of the mode excitation rates for HD 49933

The mode excitation rate $\mathcal{P}$ is inversely proportional to the mode mass $\mathcal{M}$ (see Eqs. (9), (2) and (2)). This is why we can derive $\mathcal{M}$ and $\mathcal{M}\,\mathcal{P}$ separately in order to derive $\mathcal{P}$ for HD 49933.

A.1. Derivation of $\mathcal{M}\,\mathcal{P}$

As pointed out in Sect. 3.2, the kinetic flux $F_{\rm kin} = \bar{\rho}\,\tilde{u}^3$ is almost unchanged between S1 and S0 because both 3D models have the same $T_{\rm eff}$. This has also to be the case for HD 49933 (same $T_{\rm eff}$ and same log g than S0 and S1). Therefore, the calculation of $\mathcal{M}\,\mathcal{P}$ for HD 49933 relies only on the evaluation of the values reached – at a fixed mode frequency – by the source functions $\mathcal{S}_R$ and $\mathcal{S}_S$.

As seen in Sect. 3.2, $\omega_0 = k_0\,\tilde{u}$ controls the width of χ_k in a way that the source functions $\mathcal{S}_R(\omega_{\rm osc})$ and $\mathcal{S}_S(\omega_{\rm osc})$ can be seen as functions of the dimensionless ratio $\omega_{\rm osc}/\omega_0$. The variation of E with k as well as the variation of χ_k with ω/ω_0 are shown to be similar in the two 3D simulations. Furthermore, S0 and S1 have approximately the same characteristic length Λ and hence approximately the same $k_0 \equiv 2\pi/\Lambda$. Therefore, the source function $\mathcal{S}_R$ (resp. $\mathcal{S}_S$) associated with S0 only differs from that of S1 by the characteristic velocity $\tilde{u}$. This must then also be the case for HD 49933. Further, in order to evaluate the source functions in the case of HD 49933, we only need to know the factor γ by which $\tilde{u}$ is modified in HD 49933 with respect to S1 or S0. According to Eq. (5) (resp. Eq. (6)), multipling $\tilde{u}$ by γ is equivalent to replace $\mathcal{S}_R(\omega_{\rm osc})$ (reps. $\mathcal{S}_S(\omega_{\rm osc})$) by $\gamma\,\mathcal{S}_R(\omega_{\rm osc}/\gamma)$ (resp. $\gamma\,\mathcal{S}_s(\omega_{\rm osc}/\gamma)$).

Since the kinetic flux $F_{\rm kin}$ in HD 49933 must be the same for S0 or S1, the characteristic velocity $\tilde{u}$ can be derived for HD 49933 according to $\tilde{u}_*(T) = \tilde{u}_1\,\gamma_*$ with $\gamma_*(T) \equiv (\bar{\rho}_1/\bar{\rho}_*)^{1/3}$ where $\bar{\rho}_1(T)$ is the mean density stratification of S1, $\tilde{u}_1(T)$ the characteritic velocity of S1 and $\bar{\rho}_*$ the mean density of HD 49933. Once γ_* and then $\tilde{u}_*$ are derived for HD 49933, we then compute the source functions associated with HD 49933. Finally, we compute $\mathcal{M}\,\mathcal{P}$ by keeping $F_{\rm kin}$ constant. We now turn to the derivation of the factor γ_*.

A.2. Derivation of γ_*

To derive γ_* at a given T, we need to know how the mean density $\bar{\rho}$ varies with the metal abundance Z. In order to this we consider five "standard" 1D models with five different values of Z. These 1D models are built using the same physics as described in Sect. 2.3. Two of these models have the same abundance as S0 and S1. All of the 1D models have approximately the same gravity ($\log g \simeq 4.25$) and the same effective temperature ($T_{\rm eff} \simeq 6730$ K).

The set of 1D models shows that – at any given temperature within the excitation region – $\bar{\rho}$ varies with Z rather linearly. In order to derive $\bar{\rho}$ for HD 49933, we apply – at fixed T and between S0 and S1 – a linear interpolation of $\bar{\rho}(T)$ with respect to Z.

A.3. Derivation of $\mathcal{M}$

As shown in Sect. 3.2 above in the frequency domain where modes are detected in HD 49933, $\mathcal{M}$ does not change significantly between S0 and S1. This suggests that the mode masses associated with a patched 1D model with the metal abundance expected for HD 49933 would be very similar to those associated with S0 or S1. Consequently we will assume for the case of HD 49933 the same mode masses as those associated with S1, since this 3D model has a Z abundance closer to that of HD 49933.

A.4. Derivation of $\mathcal{P}$

Before deriving $\mathcal{P}$ for HD 49933, we check that, from S0 and the knowledge of $\mathcal{P}_0$, we can approximately reproduce $\mathcal{P}_1$, the mode excitation rates, associated with S1 following the procedure described above. Let $\gamma_1 \equiv (\bar{\rho}_0/\bar{\rho}_1)^{1/3}$. As seen in Fig. 3, when we multiply $\tilde{u}_0$ by $\gamma_1(T)$ we matche $\tilde{u}_1$. Then, using $\gamma_1(T)$ and following the procedure described above, we derive $\mathcal{P}_{01}$, the mode excitation rates associated with S1 but derived from S0. The result is shown in Fig. A.1. $\mathcal{P}_{01}$ matches $\mathcal{P}_1$ rather well. However, there are differences remaining in particular in the frequency domain ν=1.2-1.5 mHz. Nevertheless, the differences between $\mathcal{P}_{01}$ and $\mathcal{P}$ are in any case not significant compared to the accuracy at which the mode amplitudes are measured with the CoRoT data (see Paper II). This validates the procedure, at least at the level of the current seismic precisions.

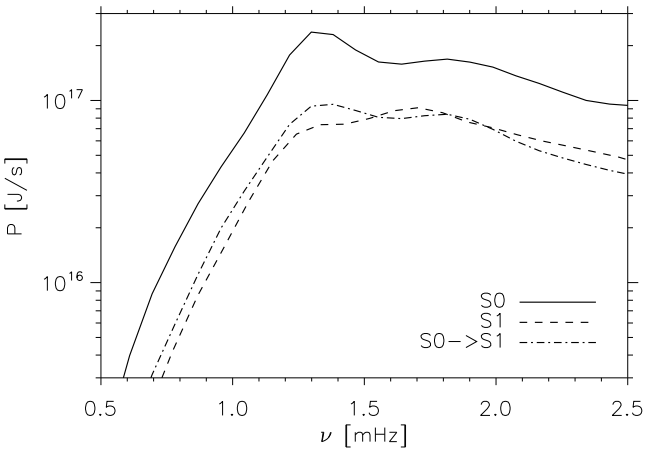

Fig. A.1. Mode excitation rates $\mathcal{P}$ as a function of the mode frequency ν. The thin dot-dashed line corresponds to $\mathcal{P}_{01}$, the mode excitation rates derived for S1 from S0 (see Appendix A4). The other lines have the same meaning as in Fig. 2.

Since the metal abundance Z of HD 49933 is closer to that of S1 than that of S0, we derive the mode excitation rates $\mathcal{P}$ associated with HD 49933 from S1 following the procedure detailled above. The result is shown in Fig. 2. As expected, the mode excitation rates $\mathcal{P}$ associated with HD 49933 lie between those of S0 and S1, while remaining closer to S1 than to S0. Note that the differences between $\mathcal{P}_1$ and the excitation rates derived for HD 49933 ($\mathcal{P}$) are of the same order as the differences seen locally between $\mathcal{P}_1$ and $\mathcal{P}_{01}$. These differences remain small compared to the current seismic precisions. On the other hand the differences

between $\mathcal{P}$ and $\mathcal{P}_0$ are significant and have an important impact on the mode amplitudes (see Paper II).